

Supplementary Information for “Complex Frequency Detection in a Subsystem”

Juntao Huang¹, Jiangping Hu^{2,3,4}, and Zhesen Yang¹

¹ Department of Physics, Xiamen University, Xiamen 361005, Fujian Province, China

² Beijing National Laboratory for Condensed Matter Physics and Institute of Physics, Chinese Academy of Sciences, Beijing 100190, China

³ School of Physical Sciences, University of Chinese Academy of Sciences, Beijing 100190, China and

⁴ New Cornerstone Science Laboratory, Beijing, 100190, China

Contents

I. Divergent behavior of the Green’s function	2
II. Complex frequency detection methods	2
A. The solution of the driving dissipative equation	2
B. Complex frequency excitation and synthesis	3
C. Complex frequency fingerprint	4
III. Derivation of the subsystem’s Green’s function	5
IV. Poles of the complex frequency Green’s function	6
References	7

I. Divergent behavior of the Green's function

This section demonstrates that the divergence of the complex frequency Green's function is uniquely associated with the existence of NHSE. Since a non-zero winding number characterizes the NHSE, this section concisely verifies that a non-zero winding number leads to the non-Bloch response or the divergent behavior of the Green's function, consistent with the conclusions presented in Fig. 1.

To examine the Green's function, we introduce $\beta = e^{ik}$ and label $\beta_{n=1,\dots,2M}$ as the roots of $\det[\omega - H(\beta)] = \frac{P(\beta,\omega)}{\beta^M} = 0$, where M represents the orbital degrees of freedom. For a given complex frequency ω , the roots can be ordered as $|\beta_1(\omega)| \leq |\beta_2(\omega)| \leq \dots \leq |\beta_M(\omega)| \leq |\beta_{M+1}(\omega)| \leq \dots \leq |\beta_{2M}(\omega)|$, where $\beta_1, \beta_2, \dots, \beta_M$ are enclosed by the generalized Brillouin Zone [1, 2]. The scaling behavior of the Green's function under OBC is described as [1, 2]

$$[G_{\text{OBC}}]_{i\alpha, j\gamma} \sim \begin{cases} \beta_{M+1}^{-(j-i)}, & i < j, \\ \beta_M^{i-j}, & i > j, \end{cases} \quad (\text{S1})$$

for large $|i - j|$, where α and γ represent orbital indices.

Additionally, the winding number is given by [3]

$$\nu(\omega) = \frac{1}{2\pi i} \int_0^{2\pi} dk \partial_k \ln \det[H_{\text{NH}}(k) - \omega], \quad (\text{S2})$$

where $H_{\text{NH}}(k)$ denotes a non-Hermitian Hamiltonian under PBC (in our case, $H_{\text{NH}}(k) = H_{S,\text{NH}}(k)$). When ω lies outside the point gap, the roots satisfy $|\beta_1(\omega)| \leq |\beta_2(\omega)| < \dots < |\beta_M(\omega)| < 1 < |\beta_{M+1}(\omega)| \leq \dots \leq |\beta_{2M}(\omega)|$ [1, 2]. Hence, the inequalities $|\beta_M(\omega)| < 1$ and $|\beta_{M+1}(\omega)| > 1$ hold for all $\nu(\omega) = 0$. In this case, we conclude that the scaling behavior of OBC Green's function will exponentially decay as i moves away from j , as illustrated in the exact result and NHA results with $\nu(\omega) = 0$ in Fig. 1 (c).

When ω lies inside the point gap, i.e., $\nu(\omega) = 1$, it follows that $|\beta_M(\omega)| > 1$ in our case ($M = 2$), indicating that the OBC Green's function exhibits divergent behavior for $i \gg j$, as illustrated in the non-Bloch region in Fig. 1 (c). Thus, the NHSE is uniquely responsible for the divergent behavior of the Green's function.

II. Complex frequency detection methods

This section reviews how complex frequency techniques, including CFE, CFS, and CFF, can be used to detect the CFGF.

A. The solution of the driving dissipative equation

The general solution of Eq. 11 can be expressed as

$$\langle \hat{\mathbf{a}}(t) \rangle = e^{-i(H_{\text{tot}} - i\gamma)t} \left[-i \int_0^t e^{i(H_{\text{tot}} - i\gamma)\tau} \mathbf{F}(\tau) d\tau + \langle \hat{\mathbf{a}}(0) \rangle \right], \quad (\text{S3})$$

where the external drive $\mathbf{F}(t) = \theta(t)e^{-i\omega t} \{F_1(0), \dots, F_N(0)\}^T$ is considered for general $\omega \in \mathbb{C}$, with $\theta(t)$ representing the step function. A straightforward integral over τ yields:

$$\begin{aligned} \langle \hat{\mathbf{a}}_\omega(t) \rangle &= e^{-i(H_{\text{tot}} - i\gamma)t} \left[-i \int_0^t e^{i(H_{\text{tot}} - i\gamma)\tau} \mathbf{F}(\tau) d\tau + \langle \hat{\mathbf{a}}(0) \rangle \right] \\ &= \frac{e^{-i\omega t} - e^{-i(H_{\text{tot}} - i\gamma)t}}{\omega + i\gamma - H_{\text{tot}}} \theta(t) \{F_1(0), \dots, F_N(0)\}^T + e^{-i(H_{\text{tot}} - i\gamma)t} \langle \hat{\mathbf{a}}(0) \rangle \\ &= G^R(\omega) (1 - e^{-i(H_{\text{tot}} - i\gamma - \omega)t}) \mathbf{F}(t) + e^{-i(H_{\text{tot}} - i\gamma - \omega)t} \text{Diag} \left(\frac{\langle \hat{a}_1(0) \rangle}{F_1(0)}, \dots, \frac{\langle \hat{a}_N(0) \rangle}{F_N(0)} \right) \mathbf{F}(t), \end{aligned} \quad (\text{S4})$$

where $G^R(\omega) = \frac{1}{\omega + i\gamma - H_{\text{tot}}}$ and $\text{Diag}(\dots)$ denotes the diagonal matrix. Notably, for $F_n(0) = 0$, the divergence ($\sim 1/(F_n(0))$) in the $\text{Diag}(\dots)$ term is canceled by the $F_n(0)$ in $\mathbf{F}(t)$. Subsequently, the response function is determined as:

$$\langle \hat{\mathbf{a}}_\omega(t) \rangle = \chi(\omega, t) \mathbf{F}(t), \quad (\text{S5})$$

with

$$\chi_{mn}(\omega, t) = G_{mn}^R(\omega) - [G^R(\omega)e^{-i(H_{tot}-i\gamma-\omega)t}]_{mn} + [e^{-i(H_{tot}-i\gamma-\omega)t}]_{mn} \langle \hat{a}_n(0) \rangle / F_n(0), \quad F_n(0) \neq 0. \quad (S6)$$

Here, the response function is well-defined when considering only the components χ_{mn} with $F_n(0) \neq 0$ and random m . Moreover, when excitation and detection are performed within subsystem S , we obtain

$$\chi_{S,ji}(\omega, t) = [G_{S,\text{eff}}^R(\omega)]_{ji} - [G^R(\omega)e^{-i(H_{tot}-i\gamma-\omega)t}]_{ji} + [e^{-i(H_{tot}-i\gamma-\omega)t}]_{ji} \langle \hat{a}_{S,i}(0) \rangle / F_{S,i}(0) \quad (S7)$$

for $i, j \in S$ and $F_{S,i}(0) \neq 0$, where $G_{S,\text{eff}}^R(\omega) = \frac{1}{\omega+i\gamma-H_S-\Sigma_S(\omega+i\gamma)}$, H_S denote the matrix form of \hat{H}_S in real space under OBC, and $\Sigma_S(\omega)$ denotes the self-energy. In this case, the component of the operator mean value takes the form $\langle \hat{a}_{S,j}(t) \rangle = \chi_{S,ji}(\omega, t)\theta(t)F_{S,i}e^{-i\omega t}$ as shown in Eq. 15 of the main text. By adjusting $F_i(0)$ or $F_{S,i}(0)$, i.e., the location of excitation, the complete information of $\chi(\omega, t)$ or $\chi_S(\omega, t)$ can be obtained. To simplify the following discussion, the initial condition $\langle \hat{a}(0) \rangle = 0$ is assumed, which does not affect the qualitative findings.

B. Complex frequency excitation and synthesis

The CFE method involves the response to an external drive $\mathbf{F}(t)$ with temporal attenuation, i.e., $\text{Im } \omega < 0$. The previous study has discussed the case of an entire non-Hermitian system, which corresponds to substituting the total Hamiltonian $H_{tot} - i\gamma$ (with trivial spectral topology under PBC) with a non-Hermitian Hamiltonian H_{NH} [4]. Then, the response function can be expressed by

$$\chi(\omega, t) = G(\omega)(1 - e^{-i(H_{\text{NH}}-\omega)t}), \quad (S8)$$

where $G(\omega) = \frac{1}{\omega - H_{\text{NH}}}$. In a dissipative system, if we denote E_s as the eigenvalue of H_{NH} that is the closest to the real axis [4], then for $\text{Im } \omega > \text{Im } E_s$, we obtain $\lim_{t \rightarrow \infty} \chi(\omega, t) = G(\omega)$. However, for $\text{Im } \omega < \text{Im } E_s$, the virtual gain [5–14] arising from the time-dependent contribution covers the information of the Green's function, leading to divergence in the response function. Therefore, $|\text{Im } E_s|$ serves as the imaginary gap of H_{NH} , characterizing the effective region for applying the CFE method.

For the subsystem S , it is evident that the response function is given by

$$\chi_{S,ji}(\omega, t) = [G_{S,\text{eff}}^R(\omega)]_{ji} - [G^R(\omega)e^{-i(H_{tot}-i\gamma-\omega)t}]_{ji}. \quad (S9)$$

We find that $\lim_{t \rightarrow \infty} \chi_{S,ji}(\omega, t) = [G_{S,\text{eff}}^R(\omega)]_{ji}$ for $\text{Im } \omega > -\gamma$. However, when $\text{Im } \omega < -\gamma$, the subsystem response function diverges as t evolves to infinity. Notably, this equation is identical to Eq. S8 when the non-Hermitian approximation is applied to subsystem S , with H_{NH} defined as $H_S - i\gamma + \Sigma_S(\omega_r + i\gamma)$, as discussed in the main text.

Besides, in dissipative systems, the detection of the response to a signal with temporal attenuation may pose a challenge in the resolution due to the low signal-to-noise ratio at a long time, hence, the method of CFS is proposed to overcome this issue [5, 6]. The basic principle of CFS is that a signal of the drive with temporal attenuation can be Fourier transformed into a series of periodic signals with varying real frequencies:

$$\mathbf{F}(t) = \frac{1}{2\pi} \int_{-\infty}^{\infty} \mathbf{f}(\omega) e^{-i\omega t} d\omega, \quad (S10)$$

where $t = 0$ is considered as the initial state. Due to the existence of a steady state under periodic signals, the response to a signal with complex frequency can be recovered through a series of responses to real frequency drives without worrying about the resolution problem. For example, consider a series of real frequency drives $\mathbf{F}_\omega(t) = e^{-i\omega t} \{F_1(0), F_2(0), \dots, F_N(0)\}^T$. By choosing $\mathbf{f}(\omega) = -i \frac{1}{\omega_c - \omega} \{F_1(0), F_2(0), \dots, F_N(0)\}^T$, we obtain

$$\begin{aligned} \frac{1}{2\pi} \int_{-\infty}^{\infty} \mathbf{f}(\omega) e^{-i\omega t} d\omega &= -\frac{i}{2\pi} \int_{-\infty}^{\infty} \frac{1}{\omega_c - \omega} \mathbf{F}_\omega(0) e^{-i\omega t} d\omega \\ &= \{F_1(0), F_2(0), \dots, F_N(0)\} e^{-i\omega_c t} \\ &= \mathbf{F}_{\omega_c}(t), \end{aligned} \quad (S11)$$

which represents a complex frequency drive. For the dissipative non-Hermitian system H_{NH} , the operator mean value under a real-frequency drive can be solved as $\langle \hat{a}_\omega(t) \rangle = G(\omega)(1 - e^{-i(H_{\text{NH}}-\omega)t})\mathbf{F}_\omega(t)$. Applying the residue theorem yields

$$\begin{aligned} -\frac{i}{2\pi} \int_{-\infty}^{\infty} \frac{1}{\omega_c - \omega} \langle \hat{a}_\omega(t) \rangle d\omega &= \frac{-i}{2\pi} \int_{-\infty}^{\infty} \frac{1}{\omega_c - \omega} G(\omega)(1 - e^{-i(H_{\text{NH}}-\omega)t})\mathbf{F}_\omega(0) e^{-i\omega t} d\omega \\ &= G(\omega_c)(1 - e^{-i(H_{\text{NH}}-\omega_c)t})\mathbf{F}_{\omega_c}(t) \\ &= \langle \hat{a}_{\omega_c}(t) \rangle. \end{aligned} \quad (S12)$$

This result can be written as

$$\langle \hat{a}_{\omega_c}(t) \rangle = \frac{1}{2\pi} \int_{-\infty}^{\infty} f(\omega) \langle \hat{a}_{\omega}(t) \rangle d\omega, \quad (\text{S13})$$

where $f(\omega) = \frac{i}{\omega - \omega_c}$. Importantly, in deriving the above result, the residue theorem is applied only once, and the term $G(\omega)(1 - e^{-i(H_{\text{nH}} - \omega)t})$ does not introduce additional poles. Expanding this term,

$$\begin{aligned} G(\omega)(1 - e^{-i(H_{\text{nH}} - \omega)t}) &= G(\omega) \left[i(H_{\text{nH}} - \omega)t - \frac{1}{2}(-it)^2(H_{\text{nH}} - \omega)^2 + \dots \right] \\ &= -it + \frac{t^2}{2}(\omega - H_{\text{nH}}) + \dots, \end{aligned} \quad (\text{S14})$$

which confirms that it does not contribute to the contour integral due to the absence of poles when applying the residue theorem.

Therefore, for subsystem S , the CFS method can also be applied, leading to the following identity

$$\langle \hat{a}_{S, \omega_c}(t) \rangle = \frac{1}{2\pi} \int_{-\infty}^{\infty} f(\omega) \langle \hat{a}_{S, \omega}(t) \rangle d\omega. \quad (\text{S15})$$

The CFS results discussed above demonstrate their equivalence with the CFE method. However, both methods cannot detect the non-Bloch response in subsystems without non-Hermitian approximation.

C. Complex frequency fingerprint

According to the response function to a real frequency drive, the CFF for the entire system is defined as [4]

$$\mathcal{G}_{\omega_r}(t) = \frac{1}{\omega_c - \omega_r + \chi^{-1}(\omega_r, t)}. \quad (\text{S16})$$

In the non-Hermitian system H_{nH} , since $\lim_{t \rightarrow \infty} \chi^{-1}(\omega_r, t) = \omega_r - H_{\text{nH}}$, we obtain $\lim_{t \rightarrow \infty} \mathcal{G}_{\omega_r}(t) = 1/(\omega_c - H_{\text{nH}})$, independent of the choice of ω_r . Consequently, by tuning the complex parameter ω across the entire complex plane, the complex frequency Green's function can be obtained. In this case, the non-Hermitian Hamiltonian is frequency-independent, which is consistent with the observable detected by the CFE and CFS methods.

The CFF for the subsystem can analogously be defined using the subsystem response function:

$$\mathcal{G}_{S, \omega_r}(t) = \frac{1}{\omega_c - \omega_r + \chi_S^{-1}(\omega_r, t)}. \quad (\text{S17})$$

To apply the CFF method to the subsystem, it is essential to outline the experimental protocol for detecting $\chi_S(\omega_r, t)$. As illustrated in Fig. S1, the subsystem S (represented by the black circle) is coupled to subsystem S' . By applying a real frequency

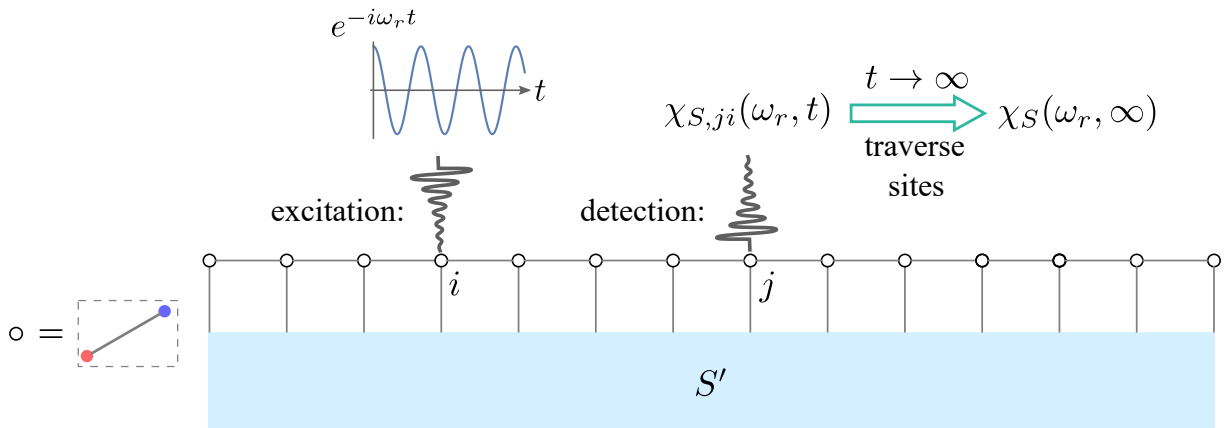


FIG. S1. The schematic diagram of the CFF method applied to subsystem S . Here, the traversed sites i, j include the orbital degrees, as illustrated by the red and blue circles in our model.

(ω_r) drive excited at site i , the component of the response function, i.e., $\chi_{S,ji}(\omega_r, t)$, can be experimentally detected. Repeating this procedure while traversing all lattice sites within S yields the complete information of $\chi_S(\omega_r, t)$. In this case, it is evident that $\lim_{t \rightarrow \infty} \chi_S^{-1}(\omega_r, t) = \omega_r - H_S + i\gamma - \Sigma_S(\omega_r + i\gamma)$, which leads to

$$\begin{aligned} \lim_{t \rightarrow \infty} \mathcal{G}_{S, \omega_r}(t) &= G_{S, \text{eff}}^{\text{CFE}}(\omega_c, \omega_r) \\ &= \frac{1}{\omega_c + i\gamma - H_S - \Sigma_S(\omega_r + i\gamma)}, \end{aligned} \quad (\text{S18})$$

where the double frequency Green's function defined above under OBC depends on the specific real frequency ω_r , with the result under PBC given in Eq. 20. As discussed aforementioned, this result being an experimental observable is consistent with the Green's function under non-Hermitian approximation at ω_r , exhibiting the non-Bloch response and showing distinct outcomes from CFE and CFS methods.

III. Derivation of the subsystem's Green's function

This section outlines the derivation of the analytic form of the subsystem's Green's function with a frequency-dependent self-energy. The discussion begins by considering the entire system under PBC along the x -direction and OBC along the y -direction. The analysis for OBC along the x -direction is straightforward by extension.

Notably, in the following derivation, we employ a Hermitian Fermionic system to derive the analytic form of the subsystem's Green's function. However, it is only the mathematical result (matrix representation of the Green's function) that is essential for investigating the response function solved from the bosonic-driven dissipative equation (Eq. 11 in the main text).

As introduced in the main text, we choose the one-dimensional Rice-Mele model as the subsystem Hamiltonian:

$$\hat{H}_S = \sum_k \hat{\psi}_k^\dagger H_S(k) \hat{\psi}_k, \quad (\text{S19})$$

where $\hat{\psi}_k^\dagger = (\hat{c}_{kA}^\dagger, \hat{c}_{kB}^\dagger)$, $\hat{\psi}_k = (\hat{c}_{kA}, \hat{c}_{kB})^T$ and $H_S(k) = (t_1 + t_2 \cos k) \sigma_x + t_2 \sin k \sigma_y + (\lambda \sin k - \mu_S) \sigma_z$. For the subsystem S' , with Fermion annihilation (creation) operators $\hat{d}_{\mathbf{R}}$ ($\hat{d}_{\mathbf{R}}^\dagger$) at site $\mathbf{R} = (x, y)$, a Fourier transformation along the x -direction yields operators satisfying PBC along x -direction and OBC along y , for example:

$$\hat{d}_{ky,A}^\dagger = \frac{1}{\sqrt{N_S}} \sum_{x=\text{odd}}^{2N_S-1} e^{ik(x+1)/2} \hat{d}_{\mathbf{R}}^\dagger, \quad \hat{d}_{ky,B} = \frac{1}{\sqrt{N_S}} \sum_{x=\text{even}}^{2N_S} e^{-ikx/2} \hat{d}_{\mathbf{R}}, \quad (\text{S20})$$

where x and y are labeled as shown in Fig. 2 (a). Notably, although the subsystem S' is a single-band model, it is divided into parts A and B to align with subsystem S for simplicity. The Hamiltonian for subsystem S' then becomes

$$\hat{H}_{S'} = \sum_k \sum_{y=2}^{N_y+1} \hat{\Psi}_{ky}^\dagger h_{S'}(k) \hat{\Psi}_{ky} + \sum_k \sum_{y=2}^{N_y} (t_y \hat{\Psi}_{ky}^\dagger \hat{\Psi}_{ky+1} + h.c.), \quad (\text{S21})$$

where $\hat{\Psi}_{ky}^\dagger = (\hat{d}_{ky,A}^\dagger, \hat{d}_{ky,B}^\dagger)$, $\hat{\Psi}_{ky} = (\hat{d}_{ky,A}, \hat{d}_{ky,B})^T$ and $h_{S'}(k) = (t_x + t_x \cos k) \sigma_x + t_x \sin k \sigma_y - \mu_{S'} \sigma_0$. The S - S' coupling is

$$\hat{H}_{SS'} = \sum_{xy} (T_{\mathbf{R}} \hat{c}_x^\dagger \hat{d}_{\mathbf{R}} + h.c.), \quad (\text{S22})$$

where

$$\hat{c}_{x=\text{odd}}^\dagger = \frac{1}{\sqrt{N_S}} \sum_k e^{-ik(x+1)/2} \hat{c}_{kA}^\dagger, \quad \hat{c}_{x=\text{even}}^\dagger = \frac{1}{\sqrt{N_S}} \sum_k e^{-ikx/2} \hat{c}_{kB}^\dagger, \quad (\text{S23})$$

and $T_{x=\text{odd}, y=2} = t_A$, $T_{x=\text{odd}, y \geq 2} = T_{x=\text{even}, y} = 0$. Subsequently, we can define the subsystem's Green's function as

$$\begin{aligned} G_{S, \alpha\beta}^R(k, t) &= -i\theta(t) \langle \{ \hat{c}_{k\alpha}(t), \hat{c}_{k\beta}^\dagger \} \rangle_T \\ G_{S', \alpha\beta}^R(k, y, t) &= -i\theta(t) \langle \{ \hat{d}_{ky, \alpha}(t), \hat{c}_{k\beta}^\dagger \} \rangle_T, \end{aligned} \quad (\text{S24})$$

where $\langle \dots \rangle_T$ represents thermal average. Here $\hat{O}(t) = e^{-i\hat{H}_{\text{tot}} t} \hat{O} e^{i\hat{H}_{\text{tot}} t}$ denotes the operator in the Heisenberg representation.

Using the commutation relations

$$\begin{aligned}
[\hat{c}_{k\alpha}, \hat{H}_{tot}] &= \sum_{\beta} [H_S(k)]_{\alpha\beta} \hat{c}_{k\beta} + \delta_{\alpha A} t_A \hat{d}_{k2,A}, \\
[\hat{d}_{k2,\alpha}, \hat{H}_{tot}] &= \sum_{\beta} [h_{S'}(k)]_{\alpha\beta} \hat{d}_{k2,\beta} + t_y \hat{d}_{k3,\alpha} + \delta_{\alpha A} t_A \hat{c}_{kA}, \\
[\hat{d}_{ky,\alpha}, \hat{H}_{tot}] &= \sum_{\beta} [h_{S'}(k)]_{\alpha\beta} \hat{d}_{ky,\beta} + (t_y \hat{d}_{ky-1,\alpha} + t_y \hat{d}_{ky+1,\alpha}), \quad y \geq 3
\end{aligned} \tag{S25}$$

the equations of motion for the Green's function in the frequency domain are:

$$\begin{aligned}
\omega G_S^R(k, \omega) &= \mathbf{I} + H_S(k) G_S^R(k, \omega) + \text{Diag}(t_A, 0) G_{S'S}^R(k, 2, \omega), \\
\omega G_{S'S}^R(k, 2, \omega) &= h_{S'}(k) G_{S'S}^R(k, 2, \omega) + T^\dagger G_{S'S}^R(k, 3, \omega) + \text{Diag}(t_A, 0) G_S^R(k, \omega), \\
\omega G_{S'S}^R(k, n, \omega) &= h_{S'}(k) G_{S'S}^R(k, n, \omega) + T G_{S'S}^R(k, n-1, \omega) + T^\dagger G_{S'S}^R(k, n+1, \omega), \quad (n \geq 3).
\end{aligned} \tag{S26}$$

Here $T = t_y \mathbf{I}$ denote the inter-layer coupling in S' . Consequently, we obtain

$$G_S^R(k, \omega) = \frac{1}{\omega - H_S(k) + i\gamma - \Sigma_S(k, \omega + i\gamma)}, \tag{S27}$$

where $\gamma > 0$ is introduced in the standard form of the retarded Green's function. By defining a $H_{\text{eff}}(k, \omega)$, the Green's function can be relabeled as $G_{S, \text{eff}}^R(k, \omega)$, as given in Eq. 5 and Eq. 6 in the main text. Here, the self-energy is expressed as

$$\Sigma_S(k, \omega) = \text{Diag}\left(\left[\frac{t_A^2}{\omega - h_{S'}(k) - T \frac{1}{\omega - h_{S'}(k) - Q_{N_y}(k, \omega)} T^\dagger}\right]_{AA}, 0\right), \tag{S28}$$

with $Q_2(k, \omega) = 0$, $Q_{n+1}(k, \omega) = T \frac{1}{\omega - h_{S'}(k) - Q_n(k, \omega)} T^\dagger$ for $n \geq 2$. This result is equivalent to $\Sigma_S^{AA}(k, \omega) = \left[\frac{t_A^2}{\omega - H_{S'}(k)}\right]_{11}$ as expressed in the main text. Numerically, $Q_{N_y}(k, \omega)$ is obtained iteratively.

Furthermore, it is easy to check that the Green's function under OBC is

$$G_{S, \text{eff}}^R(\omega) = \frac{1}{\omega - H_S + i\gamma - \Sigma_S(\omega + i\gamma)}, \tag{S29}$$

where the self-energy is given by

$$\Sigma_S(\omega) = \frac{t_A^2}{\omega - h_{S'} - T \frac{1}{\omega - h_{S'} - Q_{N_y}(\omega)} T^\dagger}, \tag{S30}$$

where $h_{S'}$ represents the real space matrix form of the one-dimensional chain along the x -direction in S' , $Q_2(\omega) = 0$, and $Q_{n+1}(\omega) = T \frac{1}{\omega - h_{S'} - Q_n(\omega)} T^\dagger$ for $n \geq 2$.

This comprehensive derivation provides a clear pathway to understanding the mathematical structure of the subsystem's Green's function, facilitating further analysis and interpretation.

IV. Poles of the complex frequency Green's function

This section analyzes the pole structures of the complex frequency Green's function, comparing cases with and without non-Hermitian approximation. For the exact case, the conventional poles for $G_{S, \text{eff}}^R(k, \omega)$ are defined through the determinant equation:

$$\det[\omega - H_{S, \text{eff}}(k, \omega)] = 0. \tag{S31}$$

Denoting ω_p as solutions to Eq. S31, we establish that

$$\omega_p(k) = \omega_r(k) - i\gamma, \tag{S32}$$

where $\omega_r \in \mathbb{R}$ satisfies

$$\det[\omega_r - H_S(k) - \Sigma_S(k, \omega_r)] = 0. \tag{S33}$$

This relationship emerges naturally because all poles of $G_{S,\text{eff}}^R(k, \omega)$ belong to those of $G^R(k, \omega)$, which exhibit imaginary parts of $-i\gamma$. This conclusion naturally extends to the OBC case.

Subsequently, we discuss the eigenvalue of $H_{S,\text{eff}}(k, \omega_r)$ for $\omega_r \in \mathbb{R}$. The central conclusion is that if we denote $\varepsilon_n(k, \omega_r)$ as the eigenvalue of $H_{S,\text{eff}}(k, \omega_r)$, then the inequality $\text{Im } \varepsilon_n(k, \omega_r) < -\gamma$ holds. To derive this, consider the matrix decomposition $\frac{1}{X+iY}$ with Hermitian X and positive-definite Hermitian Y . It is easy to check that

$$(X + iY)(Y^{-1}X \frac{1}{XY^{-1}X + Y} - i \frac{1}{XY^{-1}X + Y}) = I, \quad (\text{S34})$$

where $XY^{-1}X + Y$ is Hermitian positive-definite and invertible. This leads to the transformation

$$T \frac{1}{X + iY} T^\dagger = X' - iY', \quad (\text{S35})$$

where T here represents a Hermitian matrix ($T = t_y \mathbf{I}$ in our case), $X' = TY^{-1}X \frac{1}{XY^{-1}X + Y} T^\dagger$ is Hermitian and $Y' = T \frac{1}{XY^{-1}X + Y} T^\dagger$ is Hermitian positive-definite. Applying this framework to self-energy terms $Q_m(k, \omega_r + i\gamma)$ where $-\text{Im } Q_m(k, \omega_r + i\gamma)$ is Hermitian positive-definite, we identify $\omega_r - h_{S'}(k) - \text{Re } Q_m(k, \omega_r + i\gamma) = X$ and $i\gamma - \text{Im } Q_m(k, \omega_r + i\gamma) = iY$, yielding

$$T \frac{1}{\omega_r + i\gamma - h_{S'}(k) - Q_m(k, \omega_r + i\gamma)} T^\dagger = T \frac{1}{X + iY} T^\dagger = X' - iY' = Q_{m+1}(k, \omega_r + i\gamma), \quad (\text{S36})$$

where $-\text{Im } Q_{m+1}(k, \omega_r + i\gamma)$ remains Hermitian positive definite. Since $-\text{Im } Q_3(k, \omega_r + i\gamma) = -\text{Im } \frac{t_y^2}{\omega_r - h_{S'}(k) + i\gamma}$ is Hermitian positive definite, the iterative analysis confirms that $-\text{Im } \Sigma_S(k, \omega_r + i\gamma)$ maintains positive-definiteness in our model, enabling the decomposition

$$H_{S,\text{eff}}(k, \omega_r) = H_S(k) + X' - i(\gamma \mathbf{I} + Y'). \quad (\text{S37})$$

For normalized eigenstates $H_{S,\text{eff}}(k, \omega_r)\psi = \varepsilon(k, \omega_r)\psi$ with $\psi^\dagger\psi = 1$, we obtain

$$\begin{aligned} \text{Im } \psi^\dagger H_{S,\text{eff}}(k, \omega_r)\psi &= \text{Im } \varepsilon(k, \omega_r) \\ &= -\psi^\dagger Y' \psi - \gamma. \end{aligned} \quad (\text{S38})$$

Since Y' is positive definite, we conclude that $\text{Im } \varepsilon(k, \omega_r) < -\gamma$. As the above derivation is irrelevant to the boundary condition, the conclusion holds under OBC, explaining the imaginary gap in the non-Hermitian approximation (light yellow region as shown in Fig. 4(a)).

-
- [1] W.-T. Xue, M.-R. Li, Y.-M. Hu, F. Song, and Z. Wang, *Phys. Rev. B* **103**, L241408 (2021).
 - [2] Y.-M. Hu and Z. Wang, *Phys. Rev. Res.* **5**, 043073 (2023).
 - [3] Y. Yi and Z. Yang, *Phys. Rev. Lett.* **125**, 186802 (2020).
 - [4] J. Huang, K. Ding, J. Hu, and Z. Yang, *arXiv:2411.12577*.
 - [5] F. Guan, X. Guo, K. Zeng, S. Zhang, Z. Nie, S. Ma, Q. Dai, J. Pendry, X. Zhang, and S. Zhang, *Science* **381**, 766 (2023).
 - [6] F. Guan, X. Guo, S. Zhang, K. Zeng, Y. Hu, C. Wu, S. Zhou, Y. J. Xiang, X. Yang, and S. Zhang, *Nat. Mater.* **23**, 506 (2024).
 - [7] K. Zeng and S. Zhang, *Acta. Optica. Sinica.* **44**, 1026019 (2024).
 - [8] H. Li, A. Mekawy, A. Krasnok, and A. Alù, *Phys. Rev. Lett.* **124**, 193901 (2020).
 - [9] A. Archambault, M. Besbes, and J.-J. Greffet, *Phys. Rev. Lett.* **109**, 097405 (2012).
 - [10] K. L. Tsakmakidis, T. W. Pickering, J. M. Hamm, A. F. Page, and O. Hess, *Phys. Rev. Lett.* **112**, 167401 (2014).
 - [11] H. Tetikol and M. Aksun, *Plasmonics* **15**, 2137 (2020).
 - [12] K. Tsakmakidis and M. Wartak, *Metamaterials and Nanophotonics: Principles, Techniques and Applications* (2022).
 - [13] S. Kim, S. Lepeshov, A. Krasnok, and A. Alù, *Phys. Rev. Lett.* **129**, 203601 (2022).
 - [14] S. Kim, Y.-G. Peng, S. Yves, and A. Alù, *Phys. Rev. X* **13**, 041024 (2023).